

MindDiffuser: Controlled Image Reconstruction from Human Brain Activity with Semantic and Structural Diffusion

Yizhuo Lu*

Laboratory of Brain Atlas and
Brain-Inspired Intelligence, State Key
Laboratory of Multimodal Artificial
Intelligence Systems, CASIA
School of Future Technology,
University of Chinese Academy of
Sciences, Beijing, China
luyizhuo2023@ia.ac.cn

Changde Du*

Laboratory of Brain Atlas and
Brain-Inspired Intelligence, State Key
Laboratory of Multimodal Artificial
Intelligence Systems, CASIA
Beijing, China
changde.du@ia.ac.cn

Qiongyi zhou

Laboratory of Brain Atlas and
Brain-Inspired Intelligence, State Key
Laboratory of Multimodal Artificial
Intelligence Systems, CASIA
University of Chinese Academy of
Sciences, Beijing, China
zhouqiongyi2018@ia.ac.cn

Dianpeng Wang

School of Mathematics and Statistics
Beijing Institute of Technology
Beijing, China
wdp@bit.edu.cn

Huiguang He[†]

Laboratory of Brain Atlas and
Brain-Inspired Intelligence, State Key
Laboratory of Multimodal Artificial
Intelligence Systems, CASIA
University of Chinese Academy of
Sciences, Beijing, China
huiguang.he@ia.ac.cn

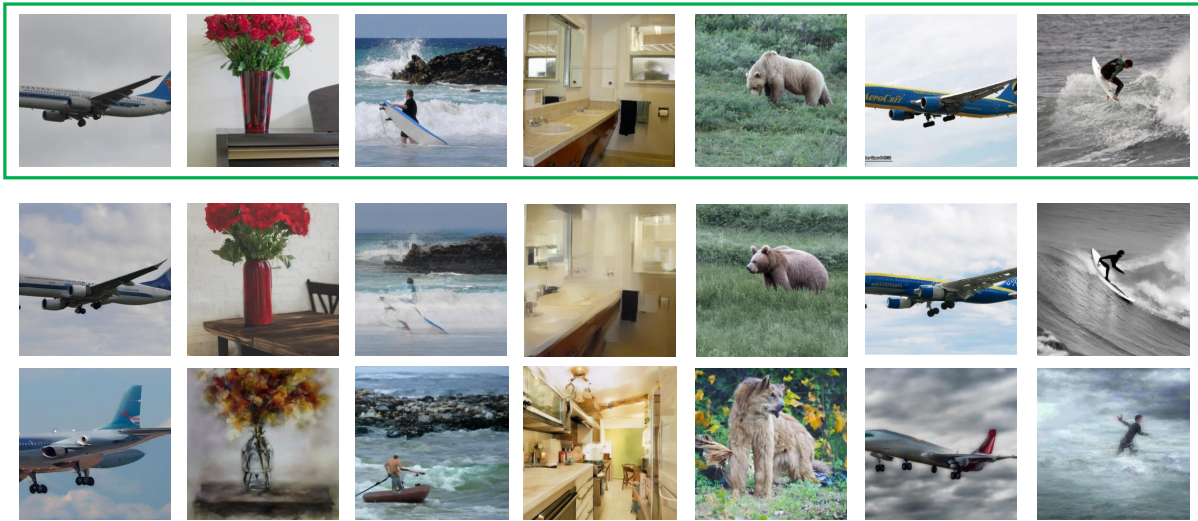


Figure 1: An overview of images reconstructed by MindDiffuser. The top row (green box) represents the image stimuli, the second row represents the upper bound of the model’s reconstruction ability, using true feature extracted from image stimuli. The last row shows our results with good alignment of both semantic and structural information to the stimuli.

ABSTRACT

Reconstructing visual stimuli from brain recordings has been a meaningful and challenging task. Especially, the achievement of precise and controllable image reconstruction bears great significance in propelling the progress and utilization of brain-computer

interfaces. Despite the advancements in complex image reconstruction techniques, the challenge persists in achieving a cohesive alignment of both semantic (concepts and objects) and structure (position, orientation, and size) with the image stimuli. To address the aforementioned issue, we propose a two-stage image reconstruction model called MindDiffuser¹. In Stage 1, the VQ-VAE latent

*Both authors contributed equally to this research.

[†] corresponding author.

¹The code has been released at: <https://github.com/ReedOnePeck/MindDiffuser>

representations and the CLIP text embeddings decoded from fMRI are put into Stable Diffusion, which yields a preliminary image that contains semantic information. In Stage 2, we utilize the CLIP visual feature decoded from fMRI as supervisory information, and continually adjust the two feature vectors decoded in Stage 1 through backpropagation to align the structural information. The results of both qualitative and quantitative analyses demonstrate that our model has surpassed the current state-of-the-art models on Natural Scenes Dataset (NSD). The subsequent experimental findings corroborate the neurobiological plausibility of the model, as evidenced by the interpretability of the multimodal feature employed, which align with the corresponding brain responses.

KEYWORDS

Probabilistic diffusion model, fMRI, Controlled Image Reconstruction, Brain-computer Interface (BCI)

1 INTRODUCTION

The human visual system possesses the exceptional ability to efficiently and robustly perceive and comprehend complex visual stimuli in the real world, which is unparalleled by current artificial intelligence systems. Understanding these brain activities and reconstructing [1] the corresponding stimuli is a critical step towards the ultimate goal of deciphering the workings of the human brain, despite its immense difficulty. With the advancement of sophisticated image generation methods and the increase in the volume of neuroimaging data, researchers are increasingly focusing on image reconstruction.

Recently, researches have revealed that deep learning frameworks exhibit a certain level of consistency with the hierarchical encoding-decoding process of the human visual system [2–4]. As a result, numerous studies have extensively employed deep neural networks (DNN) for reconstructing natural images. Based on the structure of the previous image reconstruction models, we categorize them into **optimized models** and **generative models**. The optimized model is represented by DGN [5] proposed by Shen et al., which utilizes image feature extracted from a DNN as a constraint, and optimizes the latent space of the image generator to achieve similarity with the decoded DNN feature. While this method allows for alignment of the structural information of the reconstructed images with the corresponding ones in pixel space, the absence of image priori in latent space means that optimization starting from Gaussian noise can result in indistinct outcomes and a lack of clear semantic information. The generative reconstruction models involve decoding fMRI into the latent space of models such as VAE [6], GAN [7], and Diffusion model [8], and leveraging their powerful generation capabilities to reconstruct images that are semantically similar to the original. While this paradigm enables rapid generation of realistic and semantically rich reconstruction images, the outcomes are always lacking in control over structural information.

Building upon the preceding discussions, we make the following contributions in this work:

(1) We present an image reconstruction model (MindDiffuser) that integrates the strengths of the two aforementioned paradigms and

effectively addresses their respective limitations, resulting in semantically similar and structurally aligned reconstruction outcomes. A series of detailed quantitative comparisons demonstrate that our model has surpassed the current state-of-the-art models.

(2) Our proposed two-stage image reconstruction model leverages semantic feature incorporating and structural feature aligning to achieve a remarkably powerful image reconstruction capability, as evidenced by the upper bound showcased in Figure 1. Additionally, our model can serve as a module and be combined with future advancements in more effective brain signal decoders to achieve higher-quality visual reconstruction results.

(3) Our experiments demonstrate that MindDiffuser can adapt to inter-subject variability without additional modifications. Furthermore, the visualization of feature decoding precocesses provide evidence of the model’s rationality and interpretability in neuroscience.

2 RELATED WORKS

2.1 Neural decoding and image reconstruction models

Building upon the pioneering work of Haxby [9], a multitude of neural decoding tasks with significant guiding implications have surfaced in recent decades. These tasks can be categorized into stimulus classification [9–13], stimulus identification [14–17], and stimulus reconstruction [18–23] based on their decoding objectives. Among them, stimuli reconstruction is the most alluring and demanding, and we focus on this area in the study.

Previous image reconstruction techniques utilized linear regression models to fit fMRI with manually defined image features [16, 24, 25]. The outcomes were blurry, and the features relied heavily on manual configuration. With the advent of deep learning, the use of DNNs in this domain has become more prevalent. Belyi et al. [20] and Gaziv et al. [26] employed semi-supervised learning [27] to train an Encoder-Decoder structure to reconstruct images, solving the problem of stimulus-fMRI pairs deficiency. However, the results of these models do not possess distinguishable semantic information. Du et al. [28] introduced a multi-view reconstruction model that accounts for the statistical correlation between fMRI signals and the corresponding stimuli. Du et al. [29, 30] enhances the quality of partial natural images and face reconstructions through the use of a DNN and a matrix variable Gaussian priori, employing multi-task transfer learning. Chen et al. [31] pre-trained fMRI data using a method similar to MAE [32], and fine-tuned the LDM [33] to obtain reconstructed images. Ozelik et al. [34] and Gu et al. [35] employed a self-supervised model for image instance feature extraction, followed by iterative optimization of noise and dense information using backpropagation. Subsequently, the three feature vectors were mapped from fMRI and put into IC-GAN [36] for image reconstruction.

Since the introduction of Contrastive Language-Image Pre-training (CLIP) [37], semantic information from text has been leveraged for reconstructing complex natural images. Lin et al. [38] trained a mapping model using contrastive and adversarial learning loss to align fMRI with CLIP latent representations. The mapped fMRI was then fed into StyleGAN2 [39] during the generation stage. Takagi et al. [40] achieved close-to-original reconstruction results by

mapping fMRI to the text feature c and image feature z of Stable Diffusion [33]. The most relevant work within our context is by Takagi et al. However, since no additional constraints are imposed on the generator, their resulting reconstructions lack precision in detail such as location, size, and shape.

2.2 CLIP for image generation

CLIP [37] utilizes image-text contrastive learning to endow its representation space with rich semantic information, which has been widely utilized to guide downstream image generation tasks. Here, We describe the following works according to the different roles that CLIP plays in downstream tasks.

Feed-forward image generation based on CLIP. DALL-E 2 [41] employs a prior model to transform CLIP text embeddings into corresponding image feature, which are subsequently utilized by a diffusion model to generate images. Stable Diffusion [33] utilizes CLIP text embeddings to guide the denoised process in image generation, thereby ensuring high quality output.

Besides its direct application in guiding image generation, the feature extracted by CLIP can also serve as supervisory signals for continuously refining the latent vectors of the image generator via backpropagation. This technique enables fine-grained and personalized image generation and editing.

Backward image optimization supervised by CLIP. Style-CLIP [42] begins by obtaining the latent vectors for a given image through GAN Inversion [43]. It then optimizes the latent vectors under the supervision of input text’s CLIP feature, resulting in an image that aligns with the given text. CLIPasso [44] extracts the structure and semantic information of the original image and the generated stick figure image, whose L2 distance is used as a loss function, and then optimizes the stroke parameters until convergence through backpropagation. Similar to CLIPasso, our MindDiffuser uses the low-level image feature extracted from CLIP to constrain the structural information of the reconstructed images.

The prior works leveraging the CLIP representation space mentioned in 2.1 (Lin [38], Takagi [40]) utilize the decoded CLIP feature to guide the image reconstruction process directly. To the best of our knowledge, MindDiffuser is the first approach to leverage CLIP feature as supervisory information for achieving fine-grained and controlled image reconstruction.

3 METHOD

3.1 Overview

In this section, we present **MindDiffuser**, a two-stage model for controlled image reconstruction, as shown in Figure 2. Briefly, in stage 1, we decode fMRI into CLIP text embeddings c and visual feature z in the VQ-VAE latent space. This enables the initial reconstructed images generated by Stable Diffusion to contain semantic information and fine-grained detail, thereby interpreting “**What is contained in the image ?**” In stage 2, we decode fMRI into the low-level visual feature of CLIP, and continuously optimize c and z in stage 1 by back-propagation, so that the generated images approximate the ground truth in the CLIP embedding space, thus achieving control over the structural information and deciphering “**Where are the objects in the image ?**”

3.2 Stage 1: Semantic information incorporating

Suppose that $Y \in R^{D_y \times N}$ and $X \in R^{D_x \times N}$ denote the visual stimuli and its corresponding fMRI activity patterns in the training set, respectively. And $c \in R^{D_c \times N}$, $z \in R^{D_z \times N}$ and $Z_{CLIP}^i \in R^{D_i \times N}$ denote CLIP text embeddings, VQ-VAE latent vectors and the visual feature of layer i in CLIP extracted from the training set. Here, D_j denotes the dimensions of aforementioned data, and N denotes the size of the training set. Figure 2 (a) illustrates the training process of three linear regression models: $f_c : X \mapsto c$, $f_z : X \mapsto z$ and $f_{CLIP}^i : X \mapsto Z_{CLIP}^i$ using the training set. The trained f_c and f_z are utilized to decode CLIP text embeddings c and latent vectors z of the images in test set. Subsequently, these two feature vectors are fed into Stable Diffusion, as illustrated in Figure 2 (b). To incorporate image prior into the latent space of diffusion model, decoded z undergoes a forward diffusion process for 50 steps, as outlined by equations 1 and 2, resulting in the computation of z_T .

$$q(z_t|z_{t-1}) = \mathcal{N}(z_t; \sqrt{\alpha_t}z_{t-1}, (1 - \alpha_t)I) \quad t = 0, 1, \dots, T, \quad (1)$$

$$z_T = \sqrt{\alpha_T}z + \sqrt{1 - \alpha_T}\epsilon \quad \text{and} \quad z_0 = z. \quad (2)$$

In each reverse denoising iteration, the U-Net [45] integrates decoded CLIP text embedding c into z_T by cross-attention, as defined in Equation 3.

$$\text{CrossAttention}(Q, K, V) = \text{softmax}\left(\frac{QK^T}{\sqrt{d}}\right), \quad (3)$$

$$Q = W_Q^i \cdot \phi_i(z_t), K = W_K^i \cdot c, V = W_V^i \cdot c.$$

where $\phi_i(z_t)$ represents the middle-layer feature of U-Net [45], c corresponds to the decoded CLIP text information, and W_Q^i, W_K^i, W_V^i denote the pre-trained projection matrixs. In this way, we reformulate the optimization objective of Stable Diffusion to Equation 4.

$$L_{Semantic}^t = \mathbb{E}_{z_t, \epsilon \sim \mathcal{N}(0,1), t} [\|\epsilon - \epsilon_\theta(z_t, t, c, \phi_i(z_t))\|_2^2]. \quad (4)$$

where $\epsilon_\theta(\cdot)$ is a set of denoising functions that are usually implemented as U-Net. The images generated by this process contain semantic information and fine-grained detail.

3.3 Stage 2: Structural information aligning

In stage 1, we employ the decoded CLIP text embedding c , and the VQ-VAE latent vector z to generate an initial reconstructed image \hat{Y} that contains semantic information. The CLIP visual branch, denoted as Φ , encodes high-level semantic information at the last layer and lower-level structural information such as posture and position at the shallow layers, which is revealed experimentally by Wang et al. [46]. To align the structural information of the reconstructed image with that of the original one, we devise a structural loss function based on low-level features extracted from CLIP visual encoder:

$$L_{Structure} = \sum_i \|\Phi_{CLIP}^i(\hat{Y}) - Z_{CLIP}^i\|_2^2. \quad (5)$$

As illustrated in Figure 2 (b), by iteratively backpropagating the gradients of this loss function with respect to c and z , we adjust the both components. Specifically, we begin by extracting low-level features from the preliminary image generated in the first stage using the CLIP visual encoder. Next, we compute the L2 norm

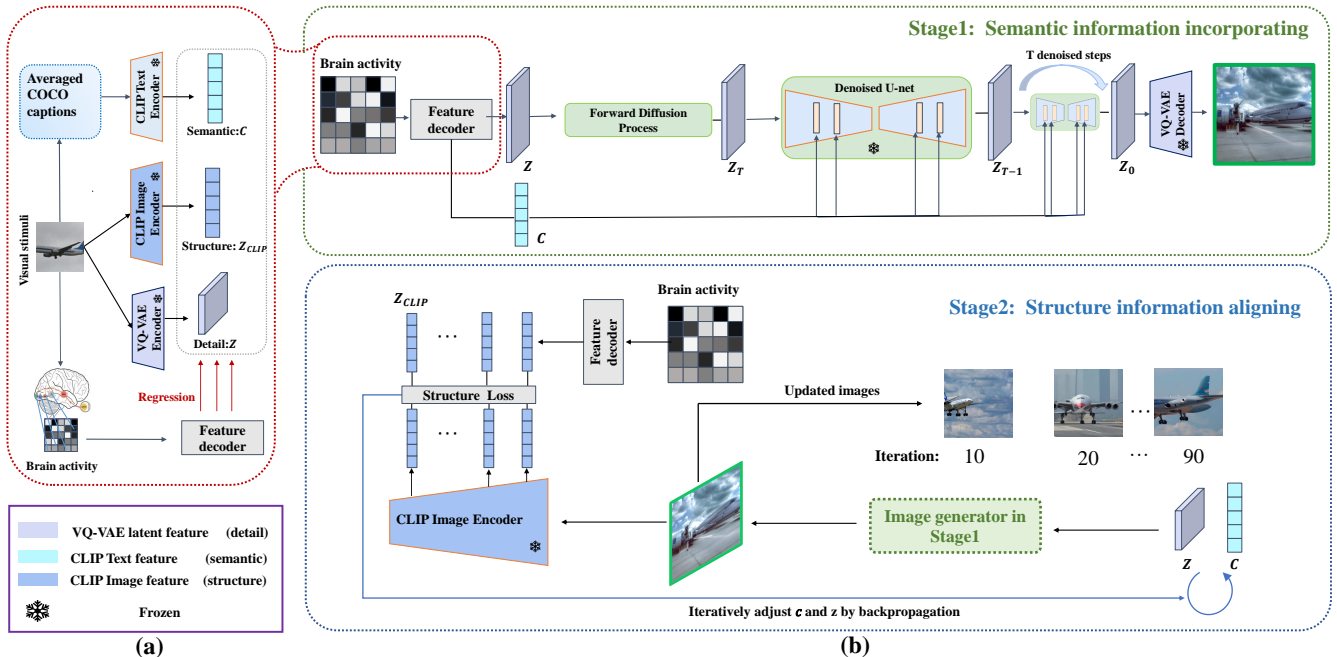


Figure 2: Schematic diagram of MindDiffuser. (a) Decoders are trained to fit fMRI with averaged CLIP text embeddings c , CLIP image feature Z_{CLIP}^i , and VQ-VAE latent feature z . (b) The two-stage image reconstruction process. In stage 1, an initial reconstructed image is generated using the decoded CLIP text feature c and VQ-VAE latent feature z . In stage 2, the decoded CLIP image feature is used as a constraint to iteratively adjust c and z until the final reconstruction result matches the original image in terms of both semantic and structure.

between the extracted features and the structural features decoded from brain signals, which serves as our structural loss function. As all operations in the model are differentiable, we adjust the c and z by backpropagation. The updated c and z are then fed into the image generator of the first stage to update the reconstructed image. This process is repeated until convergence, achieving the goal of controlling the reconstructed output.

4 EXPERIMENTS

4.1 Dataset

NSD [47] is currently the largest neuroimaging dataset bridging brain and artificial intelligence, consisting of densely sampled fMRI data from 8 subjects. Each subject viewed 9000-10000 different natural scenes (with 22000-30000 repetitions) during 30-40 MRI scanning sessions, using whole-brain gradient-echo EPI at 1.8 mm isotropic resolution and 1.6 s TR for 7T scanning. The image stimuli viewed by the subjects are obtained from the Common Objects in Context (COCO) [48] dataset and corresponding captions can be extracted using the COCO ID of the image stimuli.

To validate the stability of MindDiffuser across different subjects, we conducted experiments using fMRI-stimulus pairs from subjects 1, 2, 5, and 7 in NSD. The training set for each subject contains 8859 image stimuli and 24980 fMRI trials (with each image having up to 3 trials). Additionally, in the test set, 982 image stimuli and 2770 fMRI trials are shared among the four subjects. For fMRI data with multiple trials, we computed the average response. The properties

Dataset	Training	Test(shared)	ROIS	Subject ID	Voxels
NSD	8859	982	V1, V2, V3, hV4,	sub01	11694
			VO, PHC, MT,	sub02	9987
			MST, LO, IPS	sub05	9312
				sub07	8980

Table 1: The detail of NSD used in our experiments.

of the dataset used in our experiments have been summarized in Table 1.

4.2 Feature decoding experiments

During the image reconstruction process, we first utilize the L2-regularized Linear Regression² to decode fMRI data into three distinct spaces:

CLIP text feature space. The Stable Diffusion utilizes a CLIP text encoder with a feature space dimension of 77×768 , where 77 denotes the maximum token length and 768 represents the embedding dimension of each token. To account for the typical caption lengths in COCO, which rarely exceed 15 tokens, the first 15×768 dimensions of the flattened features are used during practical operation. The features in this space inject **semantic** information into the reconstructed images.

²We employ FastL2LiR in order to accomplish this task.

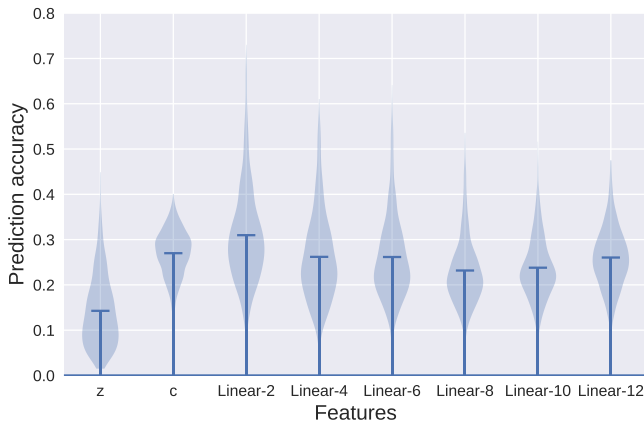


Figure 3: Decoding accuracy of each feature. The results have been averaged over 4 subjects. The blue bars represent the average prediction accuracy of all units in each feature.

VQ-VAE latent space. To integrate richer **detail**, we extract latent space feature ($1 \times 4 \times 64 \times 64$ dimensions) of the images in training set using VQ-VAE (included with Stable Diffusion) and flatten them. Subsequently, fMRI signals are mapped to this latent space.

CLIP image feature space. In order to align the **structural** information of the reconstructed images with corresponding ground truth, we choose the low-level visual feature of CLIP to control the reconstructed images, as shown in Figure 2. We choose ViT/B-32 [49] as the backbone of pre-trained CLIP, and extract features from several layers (Linear-2, Linear-4, \dots Linear-12) in the CLIP visual branch. These layers have 38400 dimensions each. Due to the potential impact of those low-accuracy feature dimensions in the decoding process, we first calculate the accuracy (Pearson correlation coefficient) of the CLIP features for each dimension in the training set using a 5-fold cross-validation. We then select the top $k\%$ of features based on their predictive accuracy and re-fit these features using all the training data. During the reconstruction of images on the test set, only these $k\%$ of features are used to guide the alignment of the original and reconstructed images. In this paper, we set $k=25$, and the methodology for selecting k is elaborated in Appendix B.

The decoding accuracy³ (Pearson correlation coefficient) of the three aforementioned features is presented in Figure 3.

4.3 Image reconstruction from decoded features

Overview of our reconstruction results. Following the process in Figure 2, some of the images reconstructed by MindDiffuser are shown in Figure 1. The upper bound illustrated in Figure 1 evinces that our proposed MindDiffuser possesses an incredibly robust reconstruction capability, wherein it can faithfully reconstruct results that are almost indistinguishable from the original images, provided truth features are given.

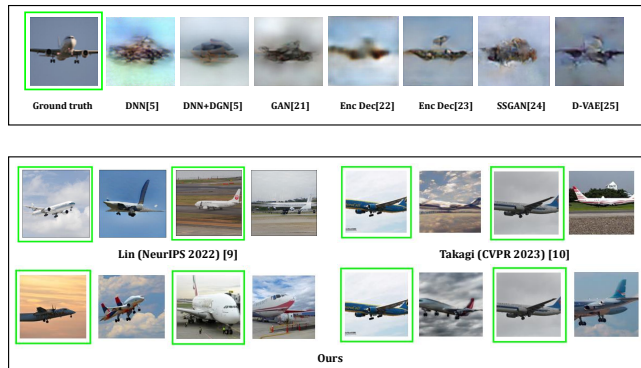


Figure 4: A brief comparison of image reconstruction results.

Given that various reconstruction models employ distinct datasets, we opt to briefly compare results fairly by utilizing the aircraft reconstruction outcomes, which are prevalent across the majority of datasets and facilitate an intuitive comparison. Figure 4 demonstrates that previous image reconstruction models, such as Shen DNN [5] and Shen GAN [5], produce outcomes that resemble the original images in terms of size, shape, and orientation, but lack semantic information necessary for recognition as an airplane⁴. Recent image reconstruction models, such as Mind Reader [38] and Takagi’s [40], incorporate text representations via multimodal pre-trained models, resulting in reconstructions with correct semantic information. However, in comparison to our MindDiffuser, their reconstructed aircrafts cannot be aligned with the original images on structural information such as shape and posture.

Comparison with state-of-the-art models. As much of the existing work on image reconstruction utilizing NSD has not yet been made fully open source, we took it upon ourselves to reproduce the results of Takagi et al. [40] and Ozcelik et al. [34] on NSD, in order to facilitate direct comparison with our findings, as shown in Figure 5. We conducted a comparative evaluation of our reconstruction outcomes with the results demonstrated by Lin [38] and Gu [35] in their published research, as delineated in Figure 6.

Methods	Semantic Similarity \uparrow	Structure Similarity \uparrow	
	CLIP Similarity	SSIM	PCC
Ozcelik [34]	0.546	0.135	0.126
Takagi (CVPR2023) [40]	0.642	0.300	0.175
Lin (NeurIPS 2022) [38]	0.578	0.243	0.102
Gu [35]	0.721	0.117	0.188
Ours	0.765	0.354	0.278

Table 2: Quantitative comparison of image reconstruction. Three metrics are utilized to evaluate the semantic and structural similarity between the original and reconstructed images. Larger metric values indicate better reconstruction quality, with the best results emphasized in bold.

³The computing process is partly implemented by MindSpore.

⁴Note that the subfigure above shows the results of an previous image reconstruction collated by Lin [38].

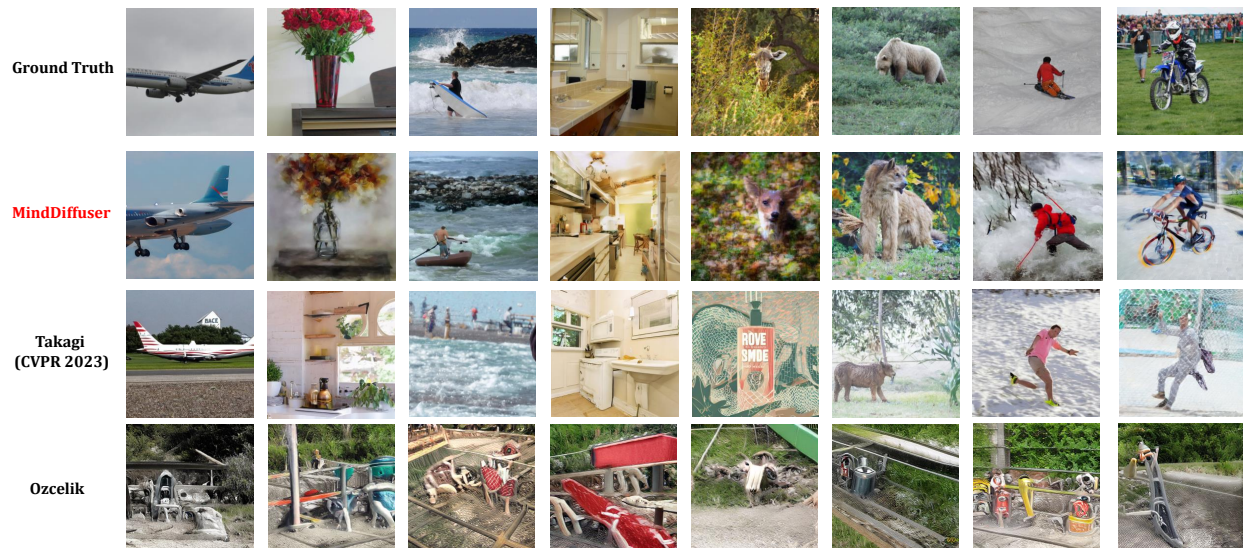


Figure 5: A comparative analysis of reconstruction models on NSD. The first line represents the image stimuli. The second line represents the results obtained using our proposed MindDiffuser. The third and fourth lines represent the results obtained by reproducing the experiment described in Takagi’s [40] paper and by using Ozcelik’s [34] provided code, respectively.

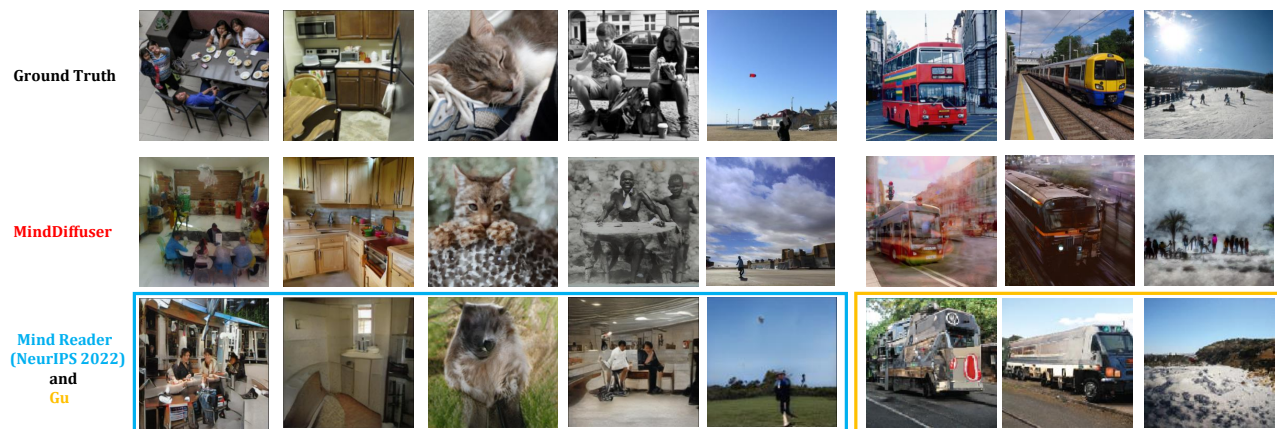


Figure 6: A comparative analysis of reconstruction models on NSD. The ground truth is presented in the first line, followed by our proposed method MindDiffuser in the second line. The reconstructed results shown in the blue box are from the work of Lin et al. [38], and we used the same training and testing data partitioning for comparative experiments. The reconstructed results presented by Gu et al. [35] are highlighted in a yellow box.

According to Figures 5 and 6, it can be observed that compared to recent work, our approach produces reconstructed results on NSD that are visually more similar to the ground truth both in terms of semantic and structure. In order to further quantitatively compare the reconstruction performance of our method with some state-of-the-art methods, we utilize three evaluation metrics to compare from both semantic and structural aspects. We use cosine similarity in the last layer of CLIP visual branch (the dimension is 512) to measure the semantic similarity between the reconstructed results and the original images. We use SSIM and per-pixel correlation coefficient (PCC) to measure the structural similarity between them.

All the three metrics range from 0 to 1, and higher values indicate better reconstruction results. For the convenience of comparison, the evaluation metrics (CLIP, SSIM, PCC) are calculated based on the reconstructed results (resized to 512×512) shown in Figures 5 and 6. The calculation results on the whole test set can be found in Table 5 in the appendix. The results from Tables 2 and 5 demonstrate that our MindDiffuser surpasses the current state-of-the-art models both semantically and structurally.

Adaptability across 4 subjects. The anatomical structure and functional connectivity of the brain vary among individuals [50], resulting in differences in the fMRI signals even when the same image stimulus is presented. To validate MindDiffuser’s ability to

adapt to inter-subject variability, we reconstruct the test images of subjects 1, 2, 5, and 7 without any additional adjustments. The results are shown in Figure 7.

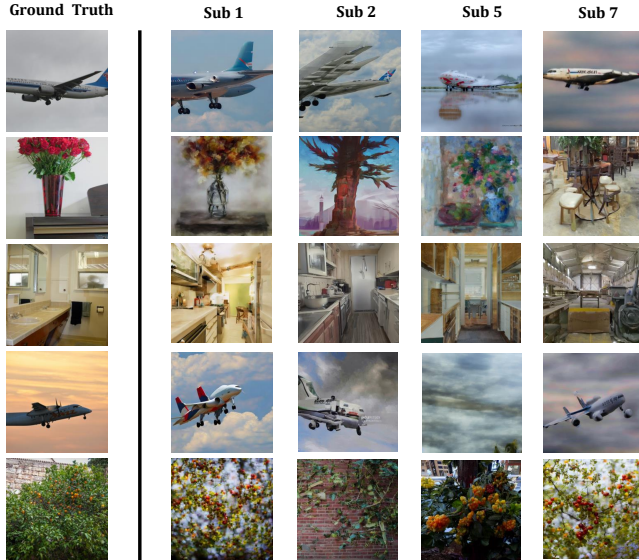


Figure 7: Reconstruction results of MindDiffuser on multiple subjects

As depicted in Figure 7, the identical image stimulus may result in different and unsatisfactory reconstruction results for some subjects due to differences in the subjective brain responses during fMRI acquisition and disparities in the accuracy of feature decoding. For instance, "flowers on the table" is erroneously reconstructed as "table and chair" in subject 7, and "aircraft at sunset" can not be reconstructed in subject 5. However, for the majority of the reconstructed images, our model achieves a satisfactory alignment with the original images in terms of both semantic and structural features for each subject, underscoring the ability of MindDiffuser to effectively accommodate variations among individuals.

4.4 Ablation study

During the feature decoding stage, we utilize the voxels from both Low-level Visual Cortex (LVC) and High-level Visual Cortex (HVC) provided in NSD. The LVC demonstrates a preference for responding to local visual information, such as shape and texture, while the HVC integrates visual elements and information over a larger receptive field, enabling the perception of global visual stimuli and semantic cognition [51, 52]. To investigate the effect of information contained within these ROIs on reconstruction results, we separately use voxels from either LVC or HVC during the decoding process. Results from the first ablation experiment are shown in Figure 8 and Table 3.

We note that LVC is more important for decoding structural and detailed information (Z_{CLIP} and z), while HVC is more important for decoding semantic information (c), which is consistent with findings in neuroscience.

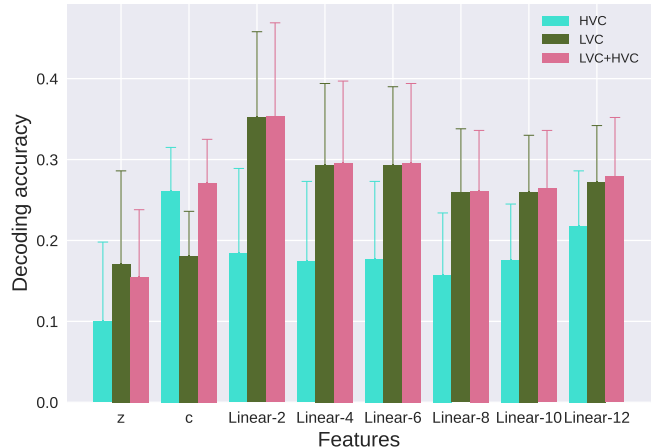


Figure 8: The decoding accuracy of different ROIs during the decoding phase. All experiments are conducted on subject 1.

Visual cortex		Semantic similarity \uparrow	Structural similarity \uparrow	
LVC	HVC	CLIP Similarity	SSIM	PCC
\checkmark		0.552	0.338	0.051
	\checkmark	0.554	0.219	0.030
\checkmark	\checkmark	0.765	0.354	0.278

Table 3: Quantitative comparison of ablation experiment results on different ROIs. The best results are emphasized in bold.

Model	Variants	Semantic similarity \uparrow	Structural similarity \uparrow	
		CLIP Similarity	SSIM	PCC
MindDiffuser	w/o c	0.549	0.346	0.218
MindDiffuser	w/o z	0.616	0.292	0.066
MindDiffuser	w/o Z_{CLIP}	0.597	0.253	0.183
MindDiffuser	completed	0.765	0.354	0.278

Table 4: Quantitative comparison of ablation experiment results on different features. The best results are emphasized in bold.

Next, we conduct ablation experiments on the three features used in MindDiffuser: semantic feature c , detail feature z , and structural feature Z_{CLIP} . The results, shown in Table 4, demonstrate that MindDiffuser outperforms other variants in reconstruction. Removing any one of the features significantly reduces the reconstruction performance.

4.5 Neuroscience interpretability

To investigate the interpretability of MindDiffuser in neuroscience, we conduct the following experiments. During the feature decoding process, we use L2-regularized linear regression model to automatically select voxels to fit three types of feature: semantic feature c , detail feature z , and structural feature Z_{CLIP} . We utilize pycortex

[53] to project the weights of each voxel in the fitted model onto the corresponding 3D coordinates in the visual cortex⁵, as shown in Figures 9, 11, 10.

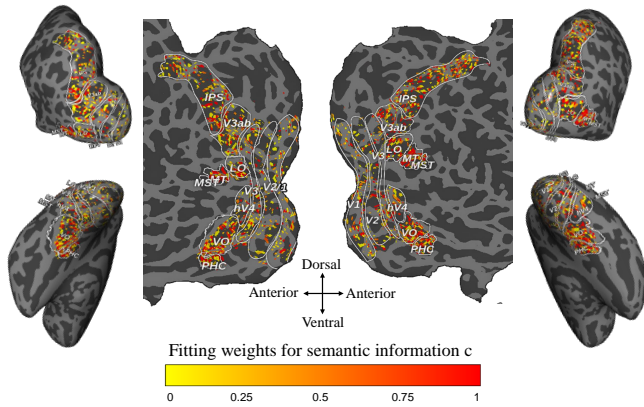


Figure 9: The importance of different ROIs of subject 1 in decoding the semantic feature c . The weights of trained linear regression model are projected onto the corresponding locations of each voxel on the cortical surface. We flatten the cortical surface into a 2D plane and discard the points with zero weights. The redder area in the figure indicates a higher weight in decoding.

The visualization from Figure 9 shows that when decoding semantic feature c , most of the selected voxels are located in IPS, LO, MT, MST, PHC, and VO that process high-level semantic information [46]. Moreover, the distribution of voxel weights within the high-level visual cortex seems to be noticeably more pronounced than that within the low-level visual cortex. Figure 10 reveals that the CLIP features Z_{CLIP} utilized for supervising the reconstruction of image structure in Stage 2 are primarily fitted by low-level visual cortex, such as V1, V2, V3, V3ab, and hV4 [46], which process local shape and texture information. We observe that in our brain decoding process, semantic feature c and structural feature Z_{CLIP} are

⁵<https://github.com/gallantlab/pycortex>

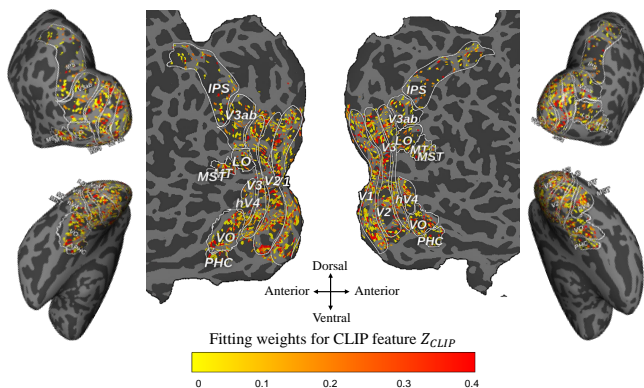


Figure 10: The importance of different ROIs of subject 1 in decoding the structural feature Z_{CLIP} .

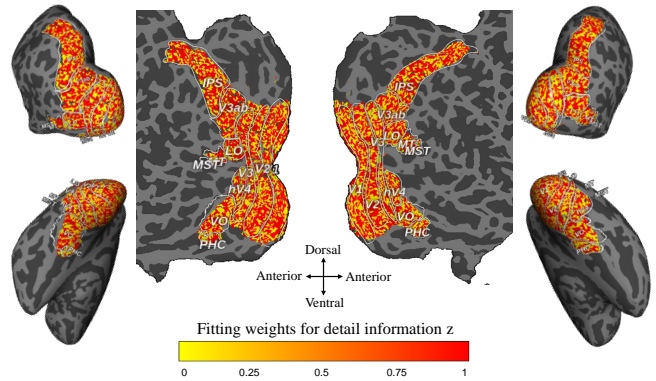


Figure 11: The importance of different ROIs of subject 1 in decoding the detail feature z .

mainly explained by high-level and low-level visual cortex separately, which is consistent with the antecedent endeavors of the predecessors [2–4, 46].

Figure 11 shows that voxels from both high-level and low-level visual cortex are involved in decoding detail feature z , with comparable weighting magnitudes. This indicates that in stage 1, decoded z enables the cross-attention mechanism to incorporate fine-grained semantic and structural detail into the reconstructed images.

The aforementioned findings corroborate the neurobiological plausibility of our model, as evidenced by the interpretability of the multimodal features employed, which align with the corresponding brain responses.

5 LIMITATIONS AND FUTURE WORK

Due to the limited temporal resolution of fMRI signals, our image reconstruction model, while effective for static images, faces challenges when directly applied to video reconstruction tasks. To address this issue, we aim to explore temporal channel modeling methods to reconstruct motion visual signals from brain. This provides a promising avenue for the reconstruction of controlled and realistic videos from brain in the future.

6 CONCLUSION

We propose a two-stage image reconstruction model, **MindDiffuser**, which aligns both semantic and structural information of the reconstructed images with the image stimuli. MindDiffuser outperforms the current state-of-the-art models qualitatively and quantitatively on NSD, given the high decoding accuracy of stage 1. Moreover, our experiments show that MindDiffuser is adaptive to inter-subject variability, achieving excellent reconstruction results for the stimuli of subjects 1, 2, 5, and 7 without any additional adjustment. Furthermore, the experiments demonstrate that the multimodal information utilized in our model can be explained by corresponding brain responses in neuroscience, thereby providing validation for the rationality of the model design. We believe that MindDiffuser plays a significant role in facilitating precise and controlled stimuli reconstruction for brain-computer interfaces.

ACKNOWLEDGMENTS

This work was supported in part by the National Key R&D Program of China 2022ZD0116500; in part by the National Natural Science Foundation of China under Grant 62206284, Grant 6202106015 and Grant 61976209; and in part by the CAAI-Huawei MindSpore Open Fund.

REFERENCES

- [1] Zarina Rakhimberdina, Quentin Jodelet, Xin Liu, and Tsuyoshi Murata. Natural image reconstruction from fMRI using deep learning: A survey. *Frontiers in neuroscience*, 15:795488, 2021.
- [2] Nicolas Pinto, David Doukhan, James J DiCarlo, and David D Cox. A high-throughput screening approach to discovering good forms of biologically inspired visual representation. *PLoS computational biology*, 5(11):e1000579, 2009.
- [3] Alex Krizhevsky, Geoffrey Hinton, et al. Learning multiple layers of features from tiny images. 2009.
- [4] Martin Schrimpf, Jonas Kubilius, Ha Hong, Najib J Majaj, Rishi Rajalingham, Elias B Issa, Kohitij Kar, Pouya Bashivan, Jonathan Prescott-Roy, Franziska Geiger, et al. Brain-score: Which artificial neural network for object recognition is most brain-like? *BioRxiv*, page 407007, 2018.
- [5] Guohua Shen, Tomoyasu Horikawa, Kei Majima, and Yukiyasu Kamitani. Deep image reconstruction from human brain activity. *PLoS computational biology*, 15(1):e1006633, 2019.
- [6] Milan Ilic. Auto-encoding variational bayes. 2019.
- [7] Ian Goodfellow, Jean Pouget-Abadie, Mehdi Mirza, Bing Xu, David Warde-Farley, Sherjil Ozair, Aaron Courville, and Yoshua Bengio. Generative adversarial networks. *Communications of the ACM*, 63(11):139–144, 2020.
- [8] Yang Song and Stefano Ermon. Generative modeling by estimating gradients of the data distribution. *Advances in neural information processing systems*, 32, 2019.
- [9] James V Haxby, M Ida Gobbini, Maura L Furey, Alumi Ishai, Jennifer L Schouten, and Pietro Pietrini. Distributed and overlapping representations of faces and objects in ventral temporal cortex. *Science*, 293(5539):2425–2430, 2001.
- [10] Marcel AJ Van Gerven, Botond Cseke, Floris P De Lange, and Tom Heskes. Efficient Bayesian multivariate fMRI analysis using a sparsifying spatio-temporal prior. *NeuroImage*, 50(1):150–161, 2010.
- [11] Saudamini Roy Damarla and Marcel Adam Just. Decoding the representation of numerical values from brain activation patterns. *Human brain mapping*, 34(10):2624–2634, 2013.
- [12] Elahe’ Yargholi and Gholam-Ali Hossein-Zadeh. Brain decoding-classification of hand written digits from fMRI data employing Bayesian networks. *Frontiers in human neuroscience*, 10:351, 2016.
- [13] Changde Du, Kaicheng Fu, Jimpeng Li, and Huiguang He. Decoding Visual Neural Representations by Multimodal Learning of Brain-Visual-Linguistic Features. *IEEE Transactions on Pattern Analysis and Machine Intelligence*, pages 1–17, 2023.
- [14] John-Dylan Haynes and Geraint Rees. Decoding mental states from brain activity in humans. *Nature reviews neuroscience*, 7(7):523–534, 2006.
- [15] Kendrick N Kay, Thomas Naselaris, Ryan J Prenger, and Jack L Gallant. Identifying natural images from human brain activity. *Nature*, 452(7185):352–355, 2008.
- [16] Thomas Naselaris, Ryan J Prenger, Kendrick N Kay, Michael Oliver, and Jack L Gallant. Bayesian reconstruction of natural images from human brain activity. *Neuron*, 63(6):902–915, 2009.
- [17] Tomoyasu Horikawa and Yukiyasu Kamitani. Generic decoding of seen and imagined objects using hierarchical visual features. *Nature communications*, 8(1):15037, 2017.
- [18] Shinji Nishimoto, An T Vu, Thomas Naselaris, Yuval Benjamini, Bin Yu, and Jack L Gallant. Reconstructing visual experiences from brain activity evoked by natural movies. *Current biology*, 21(19):1641–1646, 2011.
- [19] Guohua Shen, Kshitij Dwivedi, Kei Majima, Tomoyasu Horikawa, and Yukiyasu Kamitani. End-to-end deep image reconstruction from human brain activity. *Frontiers in Computational Neuroscience*, 13, 2019.
- [20] Roman Belyi, Guy Gaziv, Assaf Hoogi, Francesca Strappini, Tal Golan, and Michal Irani. From voxels to pixels and back: Self-supervision in natural-image reconstruction from fMRI. *Advances in Neural Information Processing Systems*, 32, 2019.
- [21] Guy Gaziv, Roman Belyi, Niv Granot, Assaf Hoogi, Francesca Strappini, Tal Golan, and Michal Irani. Self-supervised natural image reconstruction and rich semantic classification from brain activity. *bioRxiv*, 6(9):2020, 2020.
- [22] Tao Fang, Yu Qi, and Gang Pan. Reconstructing perceptive images from brain activity by shape-semantic GAN. *Advances in Neural Information Processing Systems*, 33:13038–13048, 2020.
- [23] Ziqi Ren, Jie Li, Xuotong Xue, Xin Li, Fan Yang, Zhicheng Jiao, and Xinbo Gao. Reconstructing seen image from brain activity by visually-guided cognitive representation and adversarial learning. *NeuroImage*, 228:117602, 2021.
- [24] KN Kay, Naselaris T, Prenger RJ, Gallant JL. *Identifying natural images from human brain activity*. *nature*, 452:352–355, 2008.
- [25] Yusuke Fujiwara, Yoichi Miyawaki, and Yukiyasu Kamitani. Modular encoding and decoding models derived from Bayesian canonical correlation analysis. *Neural computation*, 25(4):979–1005, 2013.
- [26] Guy Gaziv, Roman Belyi, Niv Granot, Assaf Hoogi, Francesca Strappini, Tal Golan, and Michal Irani. Self-supervised natural image reconstruction and large-scale semantic classification from brain activity. *NeuroImage*, 254:119121, 2022.
- [27] Olivier Chapelle, Bernhard Scholkopf, and Alexander Zien. Semi-supervised learning (chapelle, o. et al., eds.; 2006)[book reviews]. *IEEE Transactions on Neural Networks*, 20(3):542–542, 2009.
- [28] Changde Du, Changying Du, Lijie Huang, and Huiguang He. Reconstructing perceived images from human brain activities with Bayesian deep multiview learning. *IEEE transactions on neural networks and learning systems*, 30(8):2310–2323, 2018.
- [29] Changde Du, Changying Du, Lijie Huang, and Huiguang He. Conditional generative neural decoding with structured CNN feature prediction. In *Proceedings of the AAAI Conference on Artificial Intelligence*, volume 34, pages 2629–2636, 2020.
- [30] Changde Du, Changying Du, Lijie Huang, Haibao Wang, and Huiguang He. Structured neural decoding with multitask transfer learning of deep neural network representations. *IEEE Transactions on Neural Networks and Learning Systems*, 33(2):600–614, 2020.
- [31] Zijiao Chen, Jiaxin Qing, Tiange Xiang, Wan Lin Yue, and Juan Helen Zhou. Seeing Beyond the Brain: Conditional Diffusion Model with Sparse Masked Modeling for Vision Decoding. *arXiv preprint arXiv:2211.06956*, 2022.
- [32] Kaiming He, Xinlei Chen, Saining Xie, Yanghao Li, Piotr Dollár, and Ross Girshick. Masked autoencoders are scalable vision learners. In *Proceedings of the IEEE/CVF Conference on Computer Vision and Pattern Recognition*, pages 16000–16009, 2022.
- [33] Robin Rombach, Andreas Blattmann, Dominik Lorenz, Patrick Esser, and Björn Ommer. High-resolution image synthesis with latent diffusion models. In *Proceedings of the IEEE/CVF Conference on Computer Vision and Pattern Recognition*, pages 10684–10695, 2022.
- [34] Furkan Ozcelik, Bhavin Choksi, Milad Mozafari, Leila Reddy, and Rufin Van Rullen. Reconstruction of perceived images from fMRI patterns and semantic brain exploration using instance-conditioned GANs. In *2022 International Joint Conference on Neural Networks (IJCNN)*, pages 1–8. IEEE, 2022.
- [35] Zijin Gu, Keith Jamison, Amy Kuceyeski, and Mert Sabuncu. Decoding natural image stimuli from fMRI data with a surface-based convolutional network. *arXiv preprint arXiv:2212.02409*, 2022.
- [36] Arantxa Casanova, Marlene Careil, Jakob Verbeek, Michal Drozdal, and Adriana Romero Soriano. Instance-Conditioned GAN. *Advances in Neural Information Processing Systems*, 34:27517–27529, 2021.
- [37] Alec Radford, Jong Wook Kim, Chris Hallacy, Aditya Ramesh, Gabriel Goh, Sandhini Agarwal, Girish Sastry, Amanda Askell, Pamela Mishkin, Jack Clark, et al. Learning transferable visual models from natural language supervision. In *International conference on machine learning*, pages 8748–8763. PMLR, 2021.
- [38] Sikun Lin, Thomas Sprague, and Ambuj K Singh. Mind Reader: Reconstructing complex images from brain activities. *arXiv preprint arXiv:2210.01769*, 2022.
- [39] Tero Karras, Samuli Laine, Miika Aittala, Janne Hellsten, Jaakko Lehtinen, and Timo Aila. Analyzing and improving the image quality of StyleGAN. In *Proceedings of the IEEE/CVF conference on computer vision and pattern recognition*, pages 8110–8119, 2020.
- [40] Yu Takagi and Shinji Nishimoto. High-resolution image reconstruction with latent diffusion models from human brain activity. *bioRxiv*, pages 2022–11, 2022.
- [41] Aditya Ramesh, Prafulla Dhariwal, Alex Nichol, Casey Chu, and Mark Chen. Hierarchical text-conditional image generation with CLIP latents. *arXiv preprint arXiv:2204.06125*, 2022.
- [42] Or Patashnik, Zongze Wu, Eli Shechtman, Daniel Cohen-Or, and Dani Lischinski. StyleCLIP: Text-driven manipulation of styleGAN imagery. In *Proceedings of the IEEE/CVF International Conference on Computer Vision*, pages 2085–2094, 2021.
- [43] Weihao Xia, Yulun Zhang, Yujie Yang, Jing-Hao Xue, Bolei Zhou, and Ming-Hsuan Yang. GAN Inversion: A Survey. *IEEE Transactions on Pattern Analysis and Machine Intelligence*, 2022.
- [44] Yael Vinker, Ehsan Pajouheshgar, Jessica Y Bo, Roman Christian Bachmann, Amit Haim Bermano, Daniel Cohen-Or, Amir Zamir, and Ariel Shamir. CLIPasso: Semantically-Aware Object Sketching. *ACM Transactions on Graphics (TOG)*, 41(4):1–11, 2022.
- [45] Olaf Ronneberger, Philipp Fischer, and Thomas Brox. U-net: Convolutional networks for biomedical image segmentation. In *Medical Image Computing and Computer-Assisted Intervention—MICCAI 2015: 18th International Conference, Munich, Germany, October 5–9, 2015, Proceedings, Part III*, pages 234–241. Springer, 2015.
- [46] Aria Y. Wang, Kendrick Kay, Thomas Naselaris, Michael J. Tarr, and Leila Wehbe. Incorporating natural language into vision models improves prediction and understanding of higher visual cortex. *bioRxiv*, 2022.
- [47] Emily J Allen, Ghislain St-Yves, Yihan Wu, Jesse L Breedlove, Jacob S Prince, Logan T Dowdle, Matthias Nau, Brad Caron, Franco Pestilli, Ian Charest, et al. A massive 7T fMRI dataset to bridge cognitive neuroscience and artificial intelligence. *Nature neuroscience*, 25(1):116–126, 2022.

- [48] Tsung-Yi Lin, Michael Maire, Serge Belongie, James Hays, Pietro Perona, Deva Ramanan, Piotr Dollár, and C Lawrence Zitnick. Microsoft COCO: Common objects in context. In *Computer Vision–ECCV 2014: 13th European Conference, Zurich, Switzerland, September 6–12, 2014, Proceedings, Part V 13*, pages 740–755. Springer, 2014.
- [49] Alexey Dosovitskiy, Lucas Beyer, Alexander Kolesnikov, Dirk Weissenborn, Xiuhua Zhai, Thomas Unterthiner, Mostafa Dehghani, Matthias Minderer, Georg Heigold, Sylvain Gelly, et al. An image is worth 16x16 words: Transformers for image recognition at scale. *arXiv preprint arXiv:2010.11929*, 2020.
- [50] Alexander L Cohen, Damien A Fair, Nico UF Dosenbach, Francis M Miezin, Donna Dierker, David C Van Essen, Bradley L Schlaggar, and Steven E Petersen. Defining functional areas in individual human brains using resting functional connectivity mri. *Neuroimage*, 41(1):45–57, 2008.
- [51] Daniel J Felleman and David C Van Essen. Distributed hierarchical processing in the primate cerebral cortex. *Cerebral cortex (New York, NY: 1991)*, 1(1):1–47, 1991.
- [52] Adam Gazzaley and Anna C Nobre. Top-down modulation: bridging selective attention and working memory. *Trends in cognitive sciences*, 16(2):129–135, 2012.
- [53] James S. Gao, Alexander G. Huth, Mark D. Lescroart, and Jack L. Gallant. Pycortex: an interactive surface visualizer for fmri. *Frontiers in Neuroinformatics*, 9, 2015.

A UPPER BOUND OF THE MODEL’S RECONSTRUCTION ABILITY

Our work consists of two parts. The first part involves training brain signal decoders (top left corner of Figure 2) that utilizes regression models to map brain signals to image features, such as semantic and structural features. The second part presents our innovative two-stage image reconstruction model, which does not require training. This model leverages the input image features to reconstruct the corresponding original image. Due to the impact of the accuracy of brain signal decoding on the image reconstruction quality, we directly input the real semantic (c) and structural (z_{CLIP}) features of the original images (instead of the features decoded from brain signals) into the model, considering the resulting images as the upper bound of the model’s reconstruction ability.

B THE SELECTION OF K FOR CLIP FEATURES

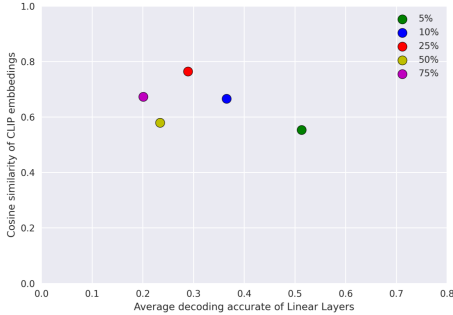


Figure 12: Illustration depicting the selection of retained percentage “k” for preserving CLIP features. (CLIP)

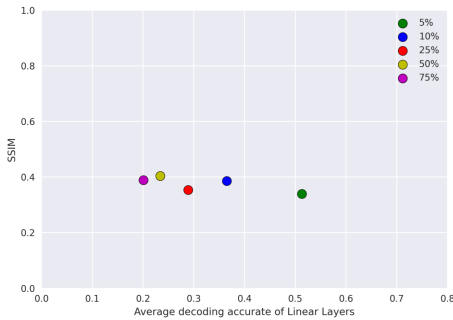


Figure 13: Illustration depicting the selection of retained percentage “k” for preserving CLIP features. (SSIM)

During feature decoding process, only those CLIP features Z_{CLIP} with prediction accuracy in the top k% are fitted. Hence, a smaller value of k leads to higher decoding accuracy, but also results in more information loss. Therefore, careful consideration is required to balance decoding accuracy and retained information when selecting the value of k. We evaluate different values of k (k=5, 10, 25, 50, and 75) using three metrics - CLIP embedding similarity, SSIM, and PCC - to measure the semantic and structural similarity between

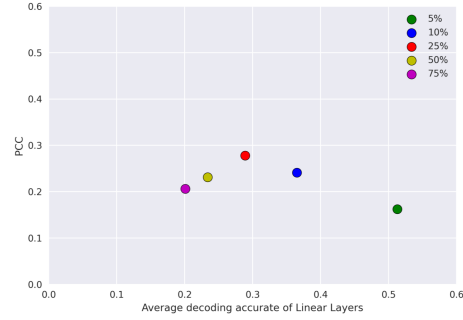


Figure 14: Illustration depicting the selection of retained percentage “k” for preserving CLIP features. (PCC)

reconstructed and original images. The evaluation is performed on the validation set (last 859 images of the training set), and the results are shown in Figures 12, 13, 14.

Based on the scatter plots, points closer to the top-right corner indicate higher decoding accuracy and better preservation of semantic and structural information. When k=25, the reconstructed results on the validation set show the maximum values for CLIP embedding similarity and PCC, with SSIM results similar to other settings. Thus, we choose k=25 in subsequent experiments.

C QUANTITATIVE COMPARISON RESULTS ON THE WHOLE TEST SET

In order to comprehensively and impartially evaluate the reconstruction performance of MindDiffuser on the NSD test set, we calculate the three metrics mentioned earlier as well as Fréchet Inception Distance (FID) ⁶ across the whole test set, as shown in Table 5.

Methods	Semantic ↑	Structure ↑		FID ↓
	CLIP Similarity	SSIM	PCC	
Ozcelik [34]	0.549	0.245	0.006	164.48
Takagis [40]	0.575	0.246	0.186	127.69
Ours (sub01)	0.603	0.238	0.241	112.83
Ours (sub02)	0.588	0.249	0.206	120.19
Ours (sub05)	0.594	0.349	0.150	116.39
Ours (sub07)	0.579	0.237	0.161	121.06
Mean	0.591	0.268	0.190	117.62

Table 5: Quantitative comparison results on the whole test set. The best results on subject 1 are emphasized in bold.

⁶<https://github.com/mseitzer/pytorch-fid>